LMTK1 regulates dendritic formation by regulating movement of Rab11A-positive endosomes

Tetsuya Takano[a], Tomoki Urushibara[a], Nozomu Yoshioka[a], Taro Saito[a], Mitsunori Fukuda[b], Mineko Tomomura[c], and Shin-ichi Hisanaga[a]

[a]Department of Biological Sciences, Tokyo Metropolitan University, Tokyo 192-0397, Japan; [b]Department of Developmental Biology and Neurosciences, Graduate School of Life Sciences, Tohoku University, Sendai 980-8578, Japan; [c]Meikai Pharmaco-Medical Laboratory, Meikai University School of Dentistry, Sakado 350-0283, Japan

ABSTRACT **Neurons extend two types of neurites—axons and dendrites—that differ in structure and function. Although it is well understood that the cytoskeleton plays a pivotal role in neurite differentiation and extension, the mechanisms by which membrane components are supplied to growing axons or dendrites is largely unknown. We previously reported that the membrane supply to axons is regulated by lemur kinase 1 (LMTK1) through Rab11A-positive endosomes. Here we investigate the role of LMTK1 in dendrite formation. Down-regulation of LMTK1 increases dendrite growth and branching of cerebral cortical neurons in vitro and in vivo. LMTK1 knockout significantly enhances the prevalence, velocity, and run length of anterograde movement of Rab11A-positive endosomes to levels similar to those expressing constitutively active Rab11A-Q70L. Rab11A-positive endosome dynamics also increases in the cell body and growth cone of LMTK1-deficient neurons. Moreover, a nonphosphorylatable LMTK1 mutant (Ser34Ala, a Cdk5 phosphorylation site) dramatically promotes dendrite growth. Thus LMTK1 negatively controls dendritic formation by regulating Rab11A-positive endosomal trafficking in a Cdk5-dependent manner, indicating the Cdk5-LMTK1-Rab11A pathway as a regulatory mechanism of dendrite development as well as axon outgrowth.**

Monitoring Editor
Kozo Kaibuchi
Nagoya University

Received: Jan 21, 2014
Revised: Mar 17, 2014
Accepted: Mar 20, 2014

INTRODUCTION

Neurons are highly polarized cells with two different types of processes called axons and dendrites. Each neuron has a single, long, unbranched process called an axon from which neurons transmit signals. Each neuron can have multiple, branched dendrites, which are the sites where neurons receive signals. Correct establishment of axons and dendrites is critical for proper neuronal network formation, and elucidating the molecular mechanisms of their formation is important for understanding neurodevelopmental disorders such as autism and schizophrenia (Bellon, 2007; Pardo and Eberhart, 2007). Neurite formation is a complicated process involving both cytoskeletal dynamics and membrane trafficking. Although axonal determination and outgrowth have been extensively studied and many critical cytoskeletal and signaling proteins have been reported (Arimura and Kaibuchi, 2007; Shelly and Poo, 2011), less is known about dendrite growth and arborization. In particular, little attention has been paid to the mechanism of membrane transport in these processes (Sann *et al.*, 2009; Yap and Winckler, 2012). In developing neurons, the supply of membrane to axons precedes its distribution to dendrites. Thus regulation of membrane trafficking is essential for accurate spatiotemporal delivery of membrane components.

Rab small GTPases are major regulatory proteins involved in membrane transport (Takai *et al.* 2001; Zerial and McBride, 2001; Stenmark, 2009). GTPases exert their regulatory control biochemically via the successive binding of GTP (active) and hydrolysis to

This article was published online ahead of print in MBoC in Press (http://www.molbiolcell.org/cgi/doi/10.1091/mbc.E14-01-0675) on March 26, 2014.

Address correspondence to: Tetsuya Takano (takano-tetsuya@ed.tmu.ac.jp), Shin-ichi Hisanaga (hisanaga-shinichi@tmu.ac.jp).

Abbreviations used: AMPA, α-amino-3-hydroxy-5-methyl-4-isoxazolepropionic acid; ca, constitutive active; Cdk5, cyclin-dependent kinase 5; DIV, days in vitro; dn, dominant negative; EGFP, enhanced green fluorescent protein; ERC, endocytic recycling compartment; LMTK1, lemur kinase 1; miRNA, microRNA; PSD95, postsynaptic density protein 95; SC, scramble sequence.

yield the GDP-bound form (inactive; Takai *et al.* 2001; Zerial and McBride, 2001; Stenmark, 2009). More than 60 members of the Rab family have been identified, and each functions in a distinct membrane compartment. Previous analysis of Rab function has been conducted mainly in nonpolarized cells. Neurons have a specialized cell shape, and membrane trafficking must operate in a region-specific manner. However, how particular membrane proteins are delivered to axons or dendrites and whether neuronal Rabs share distinct or common functions between axons and dendrites are not known.

Rab11 is a well-known regulator of recycling endosomes (Ullrich *et al.*, 1996; Sonnichsen *et al.*, 2000). In nonneuronal cells, Rab11 regulates trafficking of endocytic vesicles to the pericentriolar endocytic recycling compartment (ERC) and the recycling pathway from the ERC to the plasma membrane (Ullrich *et al.*, 1996; Sonnichsen *et al.*, 2000; Takahashi *et al.*, 2007). Rab11 has been proposed to be involved in several types of neuronal membrane transport, such as synaptic vesicle recycling in presynaptic regions, α-amino-3-hydroxy-5-methyl-4-isoxazole-propionic acid (AMPA) receptor recruitment in postsynaptic regions, and neuronal migration during development (Park *et al.*, 2004; Brown *et al.*, 2007; Sann *et al.*, 2009; Kawauchi *et al.*, 2010; Yap and Winckler, 2012). Although several reports indicate a role for Rab11 in axonal outgrowth (Ascano *et al.*, 2009; Eva *et al.*, 2010; Takano *et al.*, 2012), the role of Rab11A in dendrite outgrowth is unknown.

Lemur kinase 1 (LMTK1)/apoptosis-associated tyrosine kinase 1 (AATYK1) is an uncharacterized Ser/Thr kinase that is highly expressed in the mammalian brain (Baker *et al.*, 2001; Tomomura *et al.*, 2007). We showed that LMTK1 activity is regulated by phosphorylation at Ser-34 by cyclin-dependent kinase 5 (Cdk5)-p35 and LMTK1 regulates trafficking of recycling endosomes in CHO-K1 cells (Takano *et al.*, 2010). We recently reported that LMTK1 controls axon outgrowth in cortical neurons by modulating Rab11A function (Takano *et al.*, 2012). Here we investigate the role of LMTK1 in Rab11A-positive endosomal trafficking during dendrite formation in vitro and in vivo and the regulation of LMTK1 by Cdk5. We show that LMTK1 negatively regulates dendrite growth and arborization by modulating Rab11A-positive endosome movement.

RESULTS

Down-regulation of LMTK1 increases dendrite growth and branching

We recently reported that LMTK1 suppresses axonal outgrowth by regulating Rab11A activity in a Cdk5-dependent manner (Takano *et al.*, 2012). Here we investigate a possible role for LMTK1 in dendritic formation. We first examined the involvement of LMTK1 in dendritic growth of primary mouse cortical neurons by knocking down LMTK1 via a specific microRNA (miRNA) at 5 d in vitro (DIV)—when dendrites begin to elongate from cultured neurons after establishing an axon. LMTK1 was effectively knocked down at 7 DIV, as seen with immunoblotting (Supplemental Figure S1A) and immunostaining (Supplemental Figure S1B). We observed that LMTK1-knockdown neurons had more-elaborate dendritic processes than control neurons treated with scrambled-sequence (miRNA-SC; Figure 1, A–E). These neurites were identified as dendrites because they were labeled with the postsynaptic markers postsynaptic density protein 95 (PSD95) and AMPA receptor GluR2 (Supplemental Figure S1, C and D). We counted the neurites and evaluated arborization using Sholl analysis. The number of dendrites was elevated in LMTK1-knockdown neurons, 6.6 ± 0.1 and 5.7 ± 0.1, respectively, with the two different miRNAs, compared with 4.9 ± 0.2 in miRNA-SC control neurons (Figure 1B). Similarly, the number of branches in LMTK1-knockdown neurons, 10.5 ± 0.3 and 8.6 ± 0.5, respectively, was greater than the number, 6.9 ± 0.3, in control neurons (Figure 1C). Therefore LMTK1 knockdown increased the total primary dendrite length by ~1.7-fold (Figure 1D). The numbers of crossings at both proximal (40 μm) and distal (280 μm) lines from the cell body were greater in LMTK1-knockdown neurons than control neurons (Figure 1E). Thus LMTK1 plays a role in limiting dendrite growth and arborization of cortical neurons.

We noted in the previous report that when axon growth is stimulated by down-regulation of LMTK1, the length of other neurites was attenuated (Takano *et al.*, 2012). Therefore we next investigated how overelongation of the axon in LMTK1-knockdown neurons affects dendrite outgrowth. Three possibilities exist: 1) dendrite arborization will be suppressed due to prior consumption of membrane components by overly long axons, 2) overelongation of the axon will not affect dendrite growth, and 3) LMTK1 knockdown also stimulates dendrite outgrowth as was observed in axons. To test these possibilities, we introduced knockdown vectors into cortical neurons at 0 DIV and then analyzed dendrites after growth at 5 DIV (unpublished data) and 7 DIV (Figure 1F and Table 1). Unexpectedly, we found that cortical neurons expressing LMTK1 miRNAs extended more neurites than did those expressing mi-RNA-SC at 5 DIV (unpublished data). LMTK1 knockdown increased the number of dendrites (Figure 1G), the number of branch points (Figure 1H), the total length of primary dendrites (Figure 1I), and the number of crossings at both proximal and distal regions from the cell body (Figure 1J). These data are consistent with the third possibility—dendrite formation was enhanced after down-regulation of LMTK1 independent of prior overelongation of the axon.

Dendritic arborization is enhanced in LMTK1$^{-/-}$ mouse neurons

We confirmed the foregoing results in neurons prepared from brains of LMTK1$^{-/-}$ mice. LMTK1$^{-/-}$ neurons exhibited significantly more and longer dendritic processes (Figure 2A), larger numbers of dendrites (Figure 2B), more branches (Figure 2C), longer total primary dendrite length (Figure 2D; see Table 1 for a detailed comparison), and increased number of crossings compared with LMTK1$^{+/+}$ neurons (Figure 2E).

To confirm these findings in vivo, we compared the dendritic morphology of pyramidal neurons in the cerebral cortex of LMTK1$^{+/+}$ and LMTK1$^{-/-}$ mice with Golgi staining. We analyzed the developing brain at P7. Pyramidal neurons in layer V of the cerebral cortex have two types of dendrites—a thick apical dendrite extending toward the pial surface, and multiple basal dendrites extending basolaterally. Growth of both apical and basal dendrites was stimulated in LMTK1$^{-/-}$ brains (Figure 2F). Pyramidal neurons in LMTK1$^{-/-}$ brains had a longer apical dendrite (Figure 2G), and the number and length of the secondary dendrites increased (Figure 2, H and I). The number and length of basal dendrites also increased in LMTK1$^{-/-}$ brains (Figure 2, J and K). Thus LMTK1 negatively regulates dendrite growth in pyramidal neurons of the cerebral cortex in vivo.

During observation of LMTK1$^{-/-}$ neurons in culture, we noticed many thin protrusions along the dendrites of LMTK1$^{-/-}$ neurons (Figure 2L). The number of protrusions was 1.3 ± 0.1 in LMTK1$^{+/+}$ neurons and 5.2 ± 0.1 in LMTK1$^{-/-}$ neurons (Figure 2M). These protrusions were also observed in LMTK1-knockdown neurons (Supplemental Figure S2, A and B). They might be immature dendritic branches or spines.

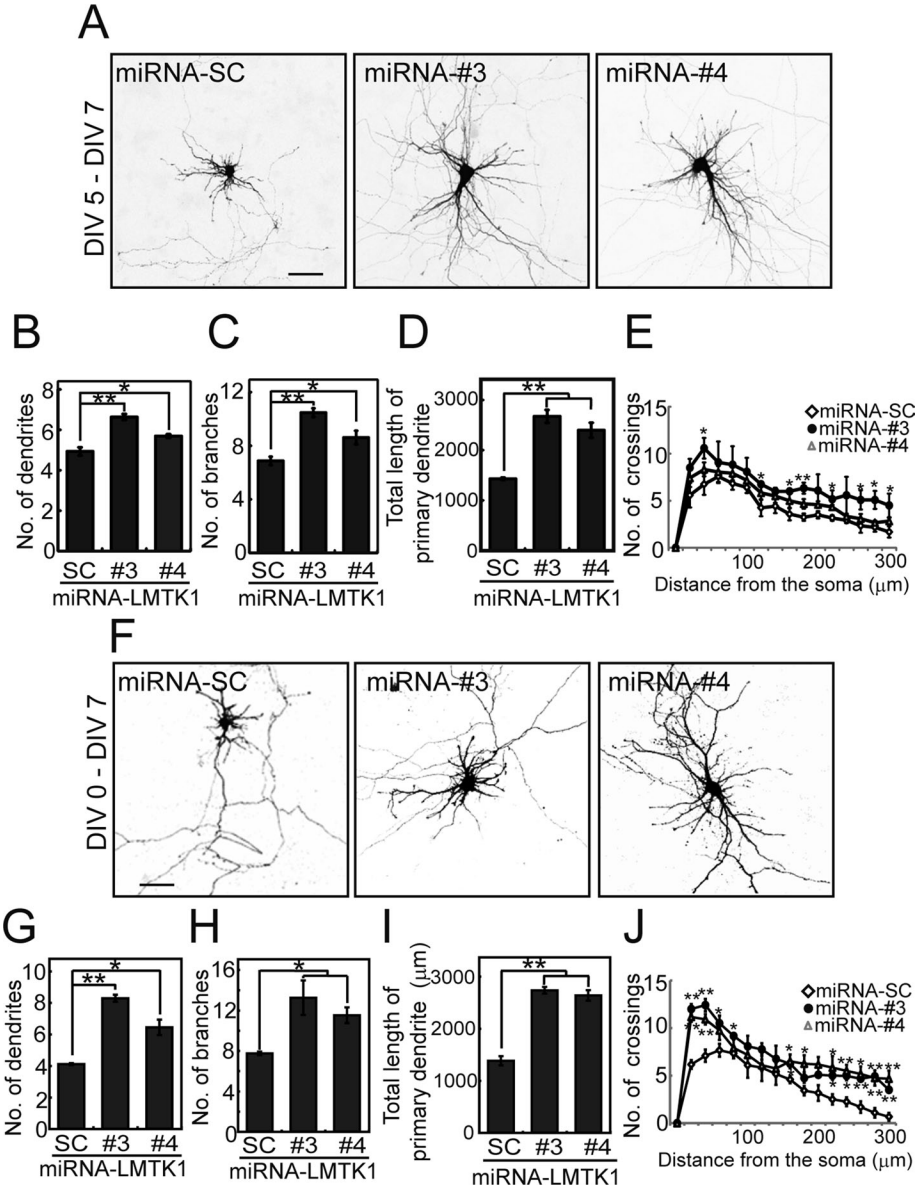

FIGURE 1: Down-regulation of LMTK1 increases dendritic arborization in cortical neurons. (A) Effect of LMTK1 knockdown by miRNAs on dendritic arborization. Cortical neurons were transfected with a plasmid encoding EmGFP-miRNA-SC, -miRNA-LMTK1#3, or -miRNA-LMTK1#4 at 5 DIV and were observed at 7 DIV. Bar, 50 μm. (B–D) The number of dendrites (B) or branches (C) and the total length of the primary dendrite (D) in miRNA-expressing neurons ($n = 30$ each for miRNA-SC and miRNA-LMTK1#3, and $n = 28$ for miRNA-LMTK1#4). (E) Sholl analysis of neurons transfected with a plasmid encoding miRNA-SC, miRNA-LMTK1#3, or miRNA-LMTK1#4 ($n = 12$ each). (F) Dendritic arborization of cortical neurons transfected with plasmids encoding miRNAs for LMTK1. Cortical neurons were transfected with a plasmid encoding miRNA-SC, miRNA-LMTK1#3, or miRNA-LMTK1#4 at 0 DIV, and neurites were analyzed at 7 DIV. Bar, 50 μm. (G–I) The number of dendrites (G), branches (H), and total length of the primary dendrite (I) in miRNA-expressing neurons ($n = 30$ for miRNA-SC, $n = 21$ for miRNA-LMTK1#3, and $n = 30$ for miRNA-LMTK1#4). (J) Sholl analysis of neurons transfected with a plasmid encoding miRNA-SC, miRNA-LMTK1#3, or miRNA-LMTK1#4 ($n = 12$ each). Data are the mean ± SEM of three independent experiments. *$p < 0.05$, **$p < 0.01$.

was found on small puncta in dendrites, which were labeled with Rab11A and partly with Rab5A but not with Rab7 (Figure 3A and Supplemental Figure S3), suggesting that LMTK1 also regulates dendrite growth via Rab11A-positive endosomes.

In the cell body, LMTK1 and Rab11A are concentrated at the ERC in the perinuclear region close to the axon, where Rab11A-positive endosomes are transported to the axon (Takano *et al.*, 2012). It is not known whether the ERC changes its location after its delivery destination changes from the axon to dendrites. We looked carefully at the localization of endogenous LMTK1 and EGFP-Rab11A in the cell body of cultured neurons at 3 and 7 DIV. Endogenous LMTK1 localized at the perinuclear region close to the base of the axon, the longest process, at both 3 and 7 DIV (Figure 3B, arrow). Rab11A accumulated at the base of the axon in primary neurons at 3 DIV, and similar localization was observed at 7 DIV (Figure 3C, arrow). This distribution was not altered in LMTK1$^{-/-}$ neurons (Figure 3C). These results suggest that the pericentriolar ERC, where LMTK1 and Rab11A accumulate, retains its position at the base of the axon in developing cultured cortical neurons.

The foregoing results indicate that recycling endosomes, which have to be delivered to dendrites, would be transported in the cell body to dendrites. We next examined how recycling endosomes move in the cell body toward dendrites from the pericentriolar ERC. We observed the movements of Rab11A-positive endosomes using real-time imaging. An example is shown in Figure 3D. In fact, endosomes moved from the pericentriolar ERC toward the dendrites in the cytoplasm between the nucleus and plasma membrane (Figure 3D, yellow arrowheads; Supplemental Videos S1 and S2). No particular accumulation or retention of endosomes was observed at the base of dendrites. Vesicles appeared to follow the same path as previous vesicles. Budding of small Rab11A-positive vesicles from the pericentriolar ERC was increased in LMTK1$^{-/-}$ neurons compared to LMTK1$^{+/+}$ neurons (Figure 3D, arrowheads in kymographs; Supplemental Video S2). These results suggest that the transport system in the cell body changes when dendrites are committed to grow.

Colocalization of LMTK1 with Rab11A in dendrites and the neuronal cell body

LMTK1 associated with Rab11A-dependent endosomes in axons (Takano *et al.*, 2012). In dendrites, we examined which Rab colocalizes with LMTK1 by coexpressing enhanced green fluorescent protein (EGFP)–Rab5A, –Rab7, or –Rab11A in cortical neurons. LMTK1

Increased prevalence, rate, and distance of anterograde movement of Rab11A-positive endosomes in dendrites of LMTK1$^{-/-}$ neurons

We analyzed how down-regulation of LMTK1 affects the movement of Rab11A-positive endosomes in primary and secondary dendrites using real-time imaging. Because the movements were similar in

Knockdown, knockout, or overexpression	Number of dendrites	Number of branches	Total dendrite length (μm)	Number of neurons analyzed
(–)	4.5 ± 1.6	7.0 ± 0.4	1298 ± 62	81
		Knockdown (5–7 DIV)[a]		
LMTK1#3	6.6 ± 0.1	10.5 ± 0.3	2673 ± 129	30
LMTK1#4	5.7 ± 0.1	8.6 ± 0.5	2397 ± 148	28
		Knockdown (0–7 DIV)[b]		
LMTK1#3	8.3 ± 0.3	13.2 ± 1.7	2734 ± 65	21
LMTK1#4	6.4 ± 0.5	11. 8 ± 0.5	2634 ±102	30
		Knockout		
$LMTK1^{+/+}$	3.4 ± 0.2	6.0 ± 0.5	1535 ±117	45
$LMTK1^{-/-}$	5.0 ± 0.5	12.6 ± 1.3	3064 ± 261	45
		Overexpression		
LMTK1-WT	4.6 ± 0.4	5.2 ± 0.6	1035 ±47	21
LMTK1-S34A	6.3 ± 0.6	9.8 ± 0.7	1465 ± 86	21
LMTK1-S34D	4.7 ± 0.1	5.2 ± 1.0	970 ± 26	21

Values are given as mean ± SEM. The original data are shown in Figures 1, 2, and 8.
[a]Cortical neurons were transfected with miRNAs at 5 DIV and observed at 7 DIV.
[b]Cortical neurons were transfected with miRNAs at 0 DIV and observed at 7 DIV.

TABLE 1: The effect of LMTK1 down-regulation or up-regulation on dendritic arborization.

primary and secondary dendrites, we followed the movement of vesicles mainly in secondary dendrites, where Rab11A-positive endosomes were easier to see due to there being fewer endosomes and thinner processes. Approximately 81% of Rab11A-positive endosomes were mobile in dendrites of $LMTK1^{+/+}$ neurons (Figure 4, A and B, and Supplemental Video S3). Among them, 37 ± 1.2% of endosomes moved from proximal to distal (anterograde), 31 ± 1.7% moved from distal to proximal (retrograde), and 32 ± 1.3% moved bidirectionally in dendrites of $LMTK1^{+/+}$ neurons (Figure 4C). Approximately 89% of Rab11A-positive endosomes were mobile in $LMTK1^{-/-}$ neurons, which was significantly higher than in $LMTK1^{+/+}$ neurons (Figure 4, A and B, and Supplemental Video S4). Further, the movement was biased toward the anterograde direction. Anterograde movement increased to 47% of total, whereas retrograde movement decreased to 19% in $LMTK1^{-/-}$ dendrites (Figure 4C). The velocities of the endosomes were 1.24 and 1.03 μm/s for anterograde and retrograde movements, respectively, in $LMTK1^{-/-}$ dendrites compared with 0.94 and 0.86 μm/s, respectively, in $LMTK1^{+/+}$ neurons (Figure 4, D and E). The most striking difference was in the run length, which is the distance traveled by the endosome without pausing during a 20-μm observation window. Although the longest run length was 4 and 5 μm for anterograde and retrograde movement, respectively, in $LMTK1^{+/+}$ neurons, it was >11 μm in both directions in $LMTK1^{-/-}$ dendrites (Figure 4, F and G, and Supplemental Video S4).

We measured several other kinetic parameters of Rab11A-positive endosomes in axons at 3 and 7 DIV, when axons alone and axons plus dendrites were growing, respectively. Approximately 71 and 60% of Rab11A-positive recycling endosomes were mobile in axons at 3 and 7 DIV in $LMTK1^{+/+}$ neurons, respectively (Figure 5B and Supplemental Video S5). Among mobile endosomes, 51 and 45% of endosomes moved anterogradely and 45 and 47% moved retrogradely at 3 and 7 DIV, respectively (Figure 5C). Approximately 4 and 8% of vesicles showed bidirectional movement at 3 and 7 DIV, respectively (Figure 5C). Thus axons at 7 DIV had fewer mobile endosomes and a lower proportion of anterograde movement than axons at 3 DIV (Table 2), indicating that trafficking of Rab11A-positive endosomes was decreased in axons when dendrites were growing.

Although we mentioned previously that axonal movements of RabA11-positive endosomes are enhanced in $LMTK1^{-/-}$ neurons, detailed analysis had not yet been performed. Here we compared their movements in wild-type (wt) and $LMTK1^{-/-}$ neurons using real-time imaging. The percentage of mobile recycling endosomes in axons at 7 DIV was ~67% in $LMTK1^{-/-}$ neurons, which was slightly higher than that in $LMTK1^{+/+}$ neurons (Figure 5B and Supplemental Video S6). Further, the proportion of anterograde movement increased slightly to 48% from 45% in $LMTK1^{+/+}$ neurons, whereas that of retrograde movement did not change (Figure 5C). The velocity of Rab11A-positive endosomes also increased to 1.18 and 1.15 μm/s in the anterograde and retrograde directions in $LMTK1^{-/-}$ axons from 0.85 and 0.92 μm/s in $LMTK1^{+/+}$ neurons, respectively (Figure 5, D and E). Thus the absence of LMTK1 increased the velocity of both anterograde and retrograde movements of recycling endosomes slightly in both dendrites and axons. However, the most obvious difference in Rab11A-positive endosomal movements between $LMTK1^{+/+}$ and $LMTK1^{-/-}$ neurons was again the run length. Although the peak of the run length was 4 μm for both anterograde and retrograde movements in $LMTK1^{+/+}$ axons, the peak run length increased to >11 μm in $LMTK1^{-/-}$ axons (Figure 5, F and G).

We compared the directionality of Rab11A-positive endosomes in dendrites and axons because the polarity of microtubules differs between axons and dendrites (Baas *et al.*, 1988; Stepanova *et al.*, 2003). In $LMTK1^{+/+}$ neurons, at times when axons (3 DIV) and dendrites (7 DIV) were actively elongating, the proportion of anterograde movement in axons and dendrites was 51 and 37%, which is higher than the 45 and 31% for retrograde movement, respectively (Table 2). In $LMTK1^{-/-}$ neurons, the proportion of anterograde movement increased to 58% in axons at 3 DIV and 47% in dendrites at 7 DIV, whereas that of retrograde movement decreased to 40%

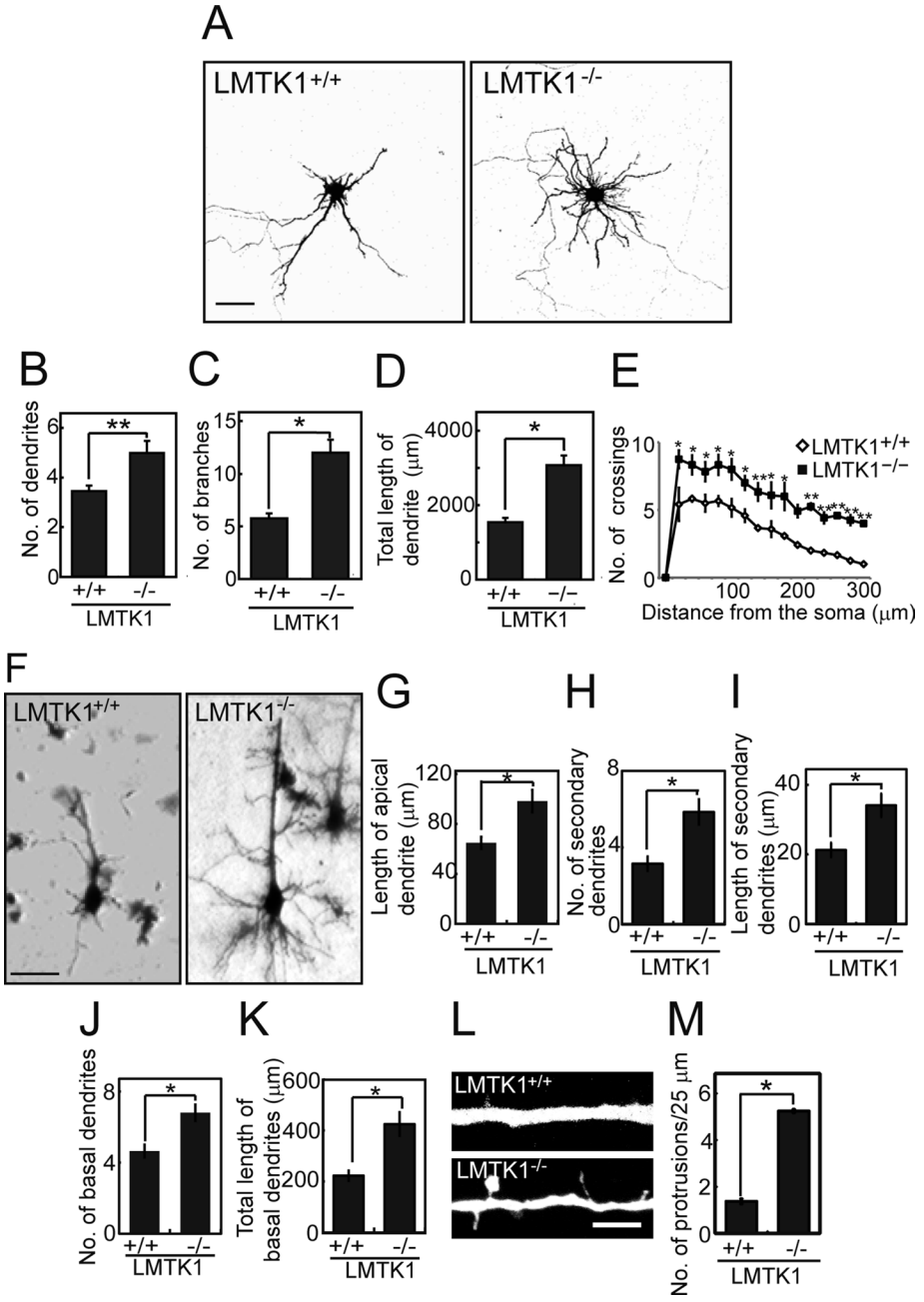

FIGURE 2: LMTK1$^{-/-}$ neurons have longer dendrites and more branches. (A) Cortical neurons from LMTK1$^{+/+}$ (left) or LMTK1$^{-/-}$ (right) brains were transfected with a plasmid encoding EGFP at 6 DIV and observed at 7 DIV. Bar, 50 μm. (B–D) The number of dendrites (B), branches (C), and total length of the primary dendrite (D) of LMTK1$^{+/+}$ or LMTK1$^{-/-}$ neurons in cultures at 7 DIV ($n = 45$ each). (E) Sholl analysis of LMTK1$^{+/+}$ or LMTK1$^{-/-}$ neurons ($n = 12$ each). (F) Golgi staining of layer V neurons in the cerebral cortex of LMTK1$^{+/+}$ (left) and LMTK1$^{-/-}$ (right) mouse brain at postnatal day 7. Bar, 40 μm. (G–I) The length of the apical dendrite (G) and the number (H) and length (I) of secondary dendrites extending from the apical dendrite ($n = 20$ each for LMTK1$^{+/+}$ and LMTK1$^{-/-}$ neurons). (J, K) The number (J) and length (K) of basal dendrites ($n = 20$ each for LMTK1$^{+/+}$ and LMTK1$^{-/-}$ neurons). (L) Protrusions along an apical dendrite of LMTK1$^{+/+}$ and LMTK1$^{-/-}$ neurons. Cultured cortical neurons from LMTK1$^{+/+}$ (top) or LMTK1$^{-/-}$ (bottom) brains were transfected with a plasmid encoding EGFP at 6 DIV and observed at 7 DIV. Bar, 5 μm. (M) The number of dendritic protrusions per 25-μm length of dendrite ($n = 30$ each for LMTK1$^{+/+}$ and LMTK1$^{-/-}$ neurons). Data are the mean ± SEM of three independent experiments. *$p < 0.05$, **$p < 0.01$, Student's t test.

and, remarkably, 19% in axons and dendrites, respectively (Table 2). Of interest, the proportion of bidirectional movement of Rab11A-positive endosomes was considerably higher in dendrites of both LMTK1$^{+/+}$ (32%) and LMTK1$^{-/-}$ (34%) neurons than in axons of LMTK1$^{+/+}$ (8%) and LMTK1$^{-/-}$ (4%) at 7 DIV (Figures 4C and 5C). The increased bidirectional movement in dendrites may reflect the mixed polarity of microtubules (Baas *et al.*, 1988; Stepanova *et al.*, 2003).

Movement of wild-type Rab11A-positive endosomes in LMTK1$^{-/-}$ neurons and constitutively active Rab11A-Q70L–positive endosomes in LMTK1$^{+/+}$ neurons

We previously showed that LMTK1 decreases the activity of Rab11A (Takano *et al.*, 2012). To assess more carefully the interaction of LMTK1 with Rab11A in endosome movement, we used constitutively active (ca) Rab11A-Q70L, which is GTPase deficient, and dominant-negative (dn) Rab11A-S25N, which is a GDP-locked mutant (Ullrich *et al.*, 1996; Ren *et al.*, 1998). We compared the movement of wtRab11A-positive endosomes in LMTK1$^{-/-}$ neurons with movement driven by caRab11A-Q70L or dnRab11A-S25N in LMTK1$^{+/+}$ neurons (Figure 6A). The caRab11A-Q70L–positive endosomes showed similar movement characteristics to wtRab11A-positive endosomes in LMTK1$^{-/-}$ neurons (Figure 6A). Approximately 85% of caRab11A-Q70L–labeled endosomes were mobile in dendrites of LMTK1$^{+/+}$ neurons, a little higher than the 78% of wtRab11A endosomes that were mobile in LMTK1$^{-/-}$ neurons (Figure 6, A and B, and Supplemental Video S7). In contrast, only 22% of dnRab11A-S25N–positive endosomes were mobile (Figure 6, A and B, and Supplemental Video S8). Among mobile caRab11A-Q70L endosomes, ~49% of endosomes showed anterograde movement, which was identical to the 49% of wtRab11A-positive endosomes in LMTK1$^{-/-}$ dendrites that were mobile but higher than the 41% of mobile wtRab11A endosomes in LMTK1$^{+/+}$ dendrites (Figure 6C). The caRab11A-Q70L vesicles moved at mean velocities of 0.99 (anterograde) and 0.96 μm/s (retrograde), which were slightly faster than the corresponding velocities of 0.85 (anterograde) and 0.85 μm/s (retrograde) for wtRab11A-labeled endosomes in LMTK1$^{+/+}$ neurons (Figure 6, E and F, and Table 2). The size of caRab11A-Q70L vesicles was 0.17 ± 0.01 μm^2, which was smaller than the 0.4 ± 0.02 μm^2 for wtRab11A-labeled endosomes in LMTK1$^{+/+}$ neurons (Figure 6D). The percentage of bidirectionally moving caRab11A-Q70L endosomes (15 ± 2.4%) was lower than the 26% for wtRab11A-labeled endosomes as estimated in the primary dendrites of LMTK1$^{-/-}$ neurons. The size of wtRab11A-positive endosomes in LMTK1$^{-/-}$ neurons was

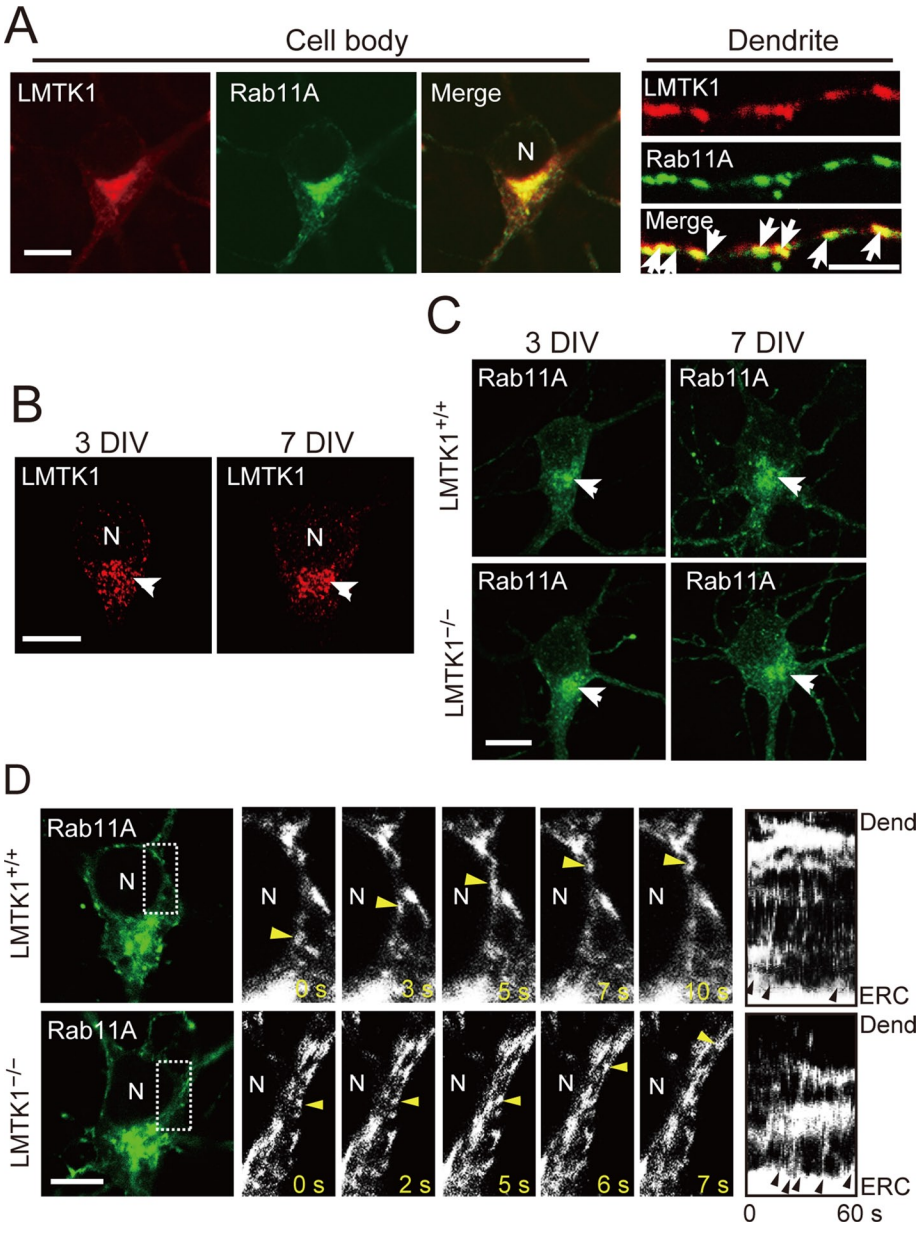

FIGURE 3: Localization of LMTK1 and Rab11A in the cell body and dendrites and movement of Rab11A-positive endosomes in the cell body of cortical neurons. (A) Colocalization of LMTK1 and Rab11A in the cell body and dendrites. Plasmids encoding LMTK1 and EGFP-Rab11A were cotransfected into primary cortical neurons at 0 DIV, and cells were visualized by immunostaining with anti-LMTK1 at 7 DIV (left). Middle, Rab11A. Right, merged image; dendrites in which LMTK1 also colocalized with Rab11A (arrows). Bar, 10 μm (cell body), 5 μm (dendrites). (B) Localization of endogenous LMTK1 at 3 (left) or 7 DIV (right). Endogenous LMTK1 was immunostained with anti-LMTK1. Bar, 10 μm. (C) Localization of Rab11A in LMTK1$^{+/+}$ (top) or LMTK1$^{-/-}$ (bottom) cortical neurons at 3 DIV (left) or 7 DIV (right). Bar, 10 μm. (D) Movement of Rab11A-positive endosomes in the cell body of LMTK1$^{+/+}$ (top) or LMTK1$^{-/-}$ (bottom) neurons. Neurons were transfected with a plasmid encoding EGFP-Rab11A at 6 DIV. Movement of Rab11A-positive endosomes was observed with real-time imaging. High-magnification images of the area indicated by the dotted line are shown for five frames with 1- to 3-s intervals. The movement of Rab11A-positive endosomes is labeled by arrowheads. Right, kymographs of Rab11A-positive endosomes budding from pericentriolar ERC and moving toward the dendrites. Arrowheads indicate budding of endosomes. N, nucleus. Bar, 20 μm.

0.16 ± 0.01 μm^2, which was comparable to the size of caRab11A-Q70L vesicles (Figure 6D). The mean velocities, 0.99 and 0.96 μm/s, for caRab11A-Q70L vesicles were slower than 1.13 and 1.16 μm/s in the anterograde and retrograde directions, respectively, in LMTK1$^{-/-}$ neurons (Figure 6, E and F). Many caRab11A-Q70L endosomes in LMTK1$^{+/+}$ neurons and wtRab11A-positive endosomes in LMTK1$^{-/-}$ neurons moved >11 μm without pausing, whereas the peak of the run length in the anterograde and retrograde directions was 5 μm for wtRab11A endosomes (Figure 6, G and H). The run length of wtRab11A-positive endosomes in LMTK1$^{-/-}$ neurons increased to >11 μm, compared with 5 μm of caRab11A-Q70L vesicles (Figure 6, G and H). Thus, as measured by several kinetic parameters, the movement of wtRab11A-positive endosomes in LMTK1$^{-/-}$ neurons was similar but not identical to that of caRab11A-Q70L-positive endosomes, suggesting that the Rab11A in LMTK1$^{-/-}$ neurons is largely in the active GTP form.

Movement of Rab11A-positive endosomes in growth cones of LMTK1$^{-/-}$ neurons

Recycling endosomes that moved to the ends of neurites may be incorporated into the plasma membrane at growth cones. However, no observations of the dynamics of Rab11A-positive endosomal movements in growth cones have been reported. Therefore we analyzed the movements of Rab11A-positive endosomes in the growth cones of dendrites in LMTK1$^{+/+}$ and LMTK1$^{-/-}$ neurons. To visualize the entire growth cone, we cotransfected a plasmid encoding a red fluorescent protein (DsRed) with a plasmid encoding EGFP-Rab11A into primary neurons. LMTK1$^{-/-}$ neurons showed a growth cone area (30 ± 4.2 μm^2) that was larger than that of LMTK1$^{+/+}$ growth cones (17 ± 2.6 μm^2; Figure 7, A and B). Rab11A-positive endosomes were smaller in LMTK1$^{-/-}$ growth cones than in LMTK1$^{+/+}$ growth cones (Figure 7C). We observed both moving and stationary endosomes in growth cones. The percentage of moving Rab11A-positive vesicles was 84 ± 0.9% in LMTK1$^{-/-}$ neurons, which was higher than in LMTK1$^{+/+}$ neurons (57 ± 3.4%; Figure 7, D and E, and Supplemental Videos S9 and S10). We frequently observed vesicles that moved to the tip of the growth cone and disappeared (Figure 7E). During a 160-s recording, 5.8 ± 0.6 Rab11A-positive endosomes disappeared at the tip of growth cones in LMTK1$^{-/-}$ neurons, whereas only 2.7 ± 0.5 were in LMTK1$^{+/+}$ growth cones (Figure 7F). In contrast, the number of vesicles entering the growth cone from the dendritic shaft was not different between LMTK1$^{-/-}$ neurons (3.3 ± 0.4) and LMTK1$^{+/+}$ neurons (3.2 ± 0.3; Figure 7G). However, the number of vesicles returning to the dendritic shaft was lower in LMTK1$^{-/-}$ neurons (1.9 ± 0.3) compared with LMTK1$^{+/+}$ neurons (2.8 ± 0.3; Figure 7H). The difference will result in

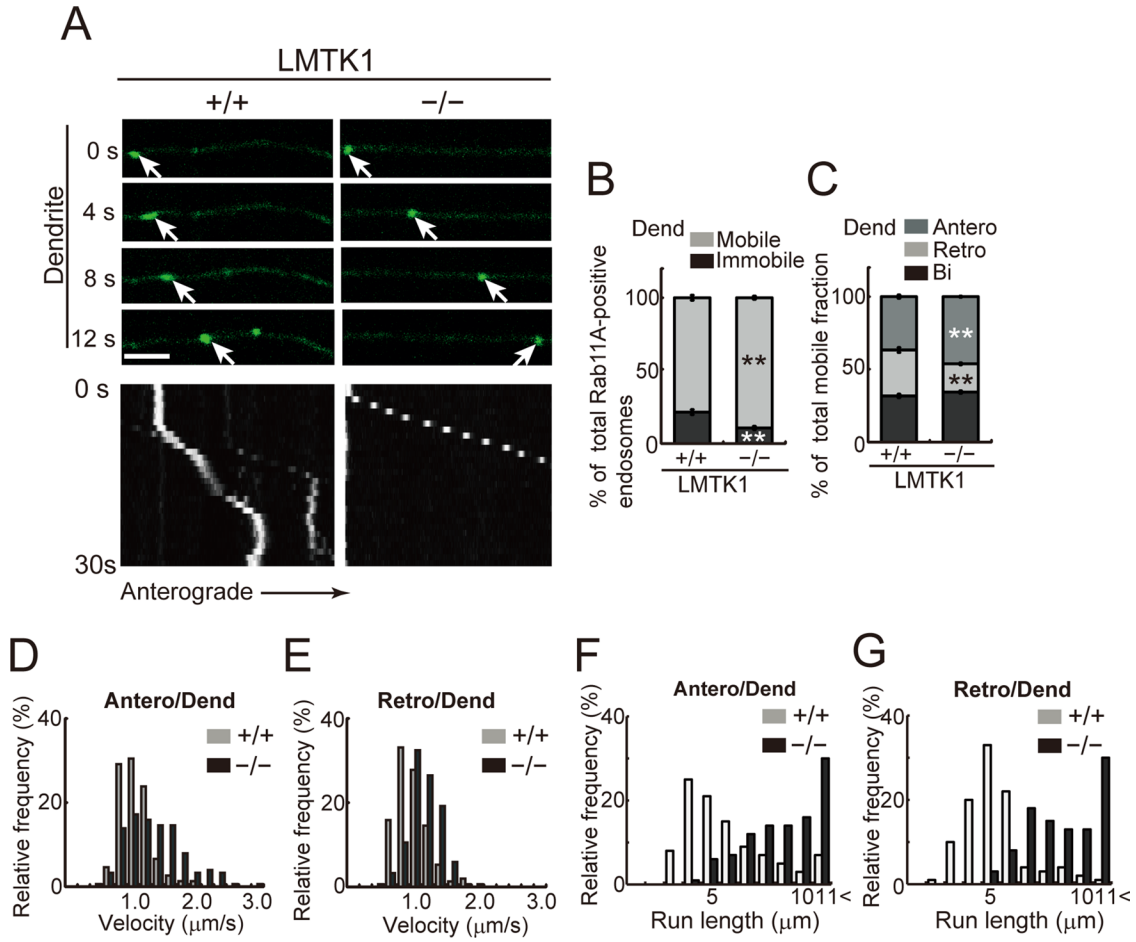

FIGURE 4: Dynamics of Rab11A-positive endosomes in dendrites of LMTK1$^{-/-}$ neurons. (A) Movement of Rab11A-positive endosomes in a dendrite of a LMTK1$^{+/+}$ or LMTK1$^{-/-}$ neuron. Neurons were transfected with a plasmid encoding EGFP-Rab11A. Movement of Rab11A-positive endosomes in secondary dendrites was observed with real-time imaging. Sequential frames for 12 s with a 4-s interval are shown for LMTK1$^{+/+}$ and LMTK1$^{-/-}$. The cell body is on the left side. The movement of a typical Rab11A-positive endosome is indicated with arrows. Bottom, kymographs of Rab11A-positive endosomes moving in dendrites. Bar, 5 μm. (B) Percentage of moving (light gray) or stationary (dark gray) Rab11A-positive endosomes in dendrites. (C) Percentage of Rab11A-positive endosomes moving anterogradely (gray), retrogradely (light gray), or bidirectionally (dark gray) in dendrites (n = 381 endosomes in LMTK1$^{+/+}$ neurons and n = 432 endosomes in LMTK1$^{-/-}$ neurons). (D, E) Velocity of Rab11A-positive endosomes in dendrites. Relative frequency of Rab11A-positive endosomes moving at the indicated velocities in the anterograde (D) or retrograde (E) direction in dendrites of LMTK1$^{+/+}$ (light gray) or LMTK1$^{-/-}$ (dark gray) neurons (n = 150 endosomes each for LMTK1$^{+/+}$ and LMTK1$^{-/-}$). (F, G) Run length of Rab11A-positive endosomes in dendrites. The distance that Rab11A-positive endosomes moved without pausing was measured in a 20-μm observation window. Relative frequency of Rab11A-positive endosomes moving at the indicated run length in the anterograde (F) or retrograde (G) direction in dendrites of LMTK1$^{+/+}$ (light gray) or LMTK1$^{-/-}$ (dark gray) neurons (n = 100 endosomes each for LMTK1$^{+/+}$ and LMTK1$^{-/-}$).

a net supply of membranes to the growth cone. These results suggest that LMTK1 also suppresses the fusion of Rab11A-positive endosomes into the tip of neurites, the final step of the recycling pathway.

Effect of phosphorylation of LMTK1 at Ser-34 on dendritic arborization

Cdk5-p35 can phosphorylate LMTK1 at Ser-34, thereby modulating LMTK1's ability to regulate axonal outgrowth (Takano *et al.*, 2012). We therefore examined whether the function of LMTK1 on dendrite arborization is also regulated by Cdk5-p35–mediated phosphorylation. The phosphorylation of LMTK1 at Ser-34 increased gradually from 3 to 9 DIV in cultured cortical neurons and then remained constant until 13 DIV, in parallel with the expression of the Cdk5 activator p35 (Supplemental Figure S4). Because our phospho–Ser-34 antibody was not sensitive enough to detect endogenous LMTK1 phosphorylation, we examined the cellular localization of phospho–Ser-34 by expressing exogenous LMTK1 in cortical neurons. Phospho-LMTK1 was abundantly expressed in the perinuclear region of the cell soma (Figure 8A, top, arrow) and was seen on small puncta in dendrites (Figure 8A, bottom). We next examined the effect of overexpressing two myc-labeled LMTK1 mutants—the S34A nonphosphorylatable form and the S34D phosphorylation mimic form—on dendritic arborization. Neurons were visualized with DsRed cotransfected with LMTK1-myc mutants. Neurons expressing LMTK1-S34A showed remarkably well-developed dendritic arborization compared with neurons expressing LMTK1-S34D or LMTK1-WT, the dendrites of which were similar to those of control

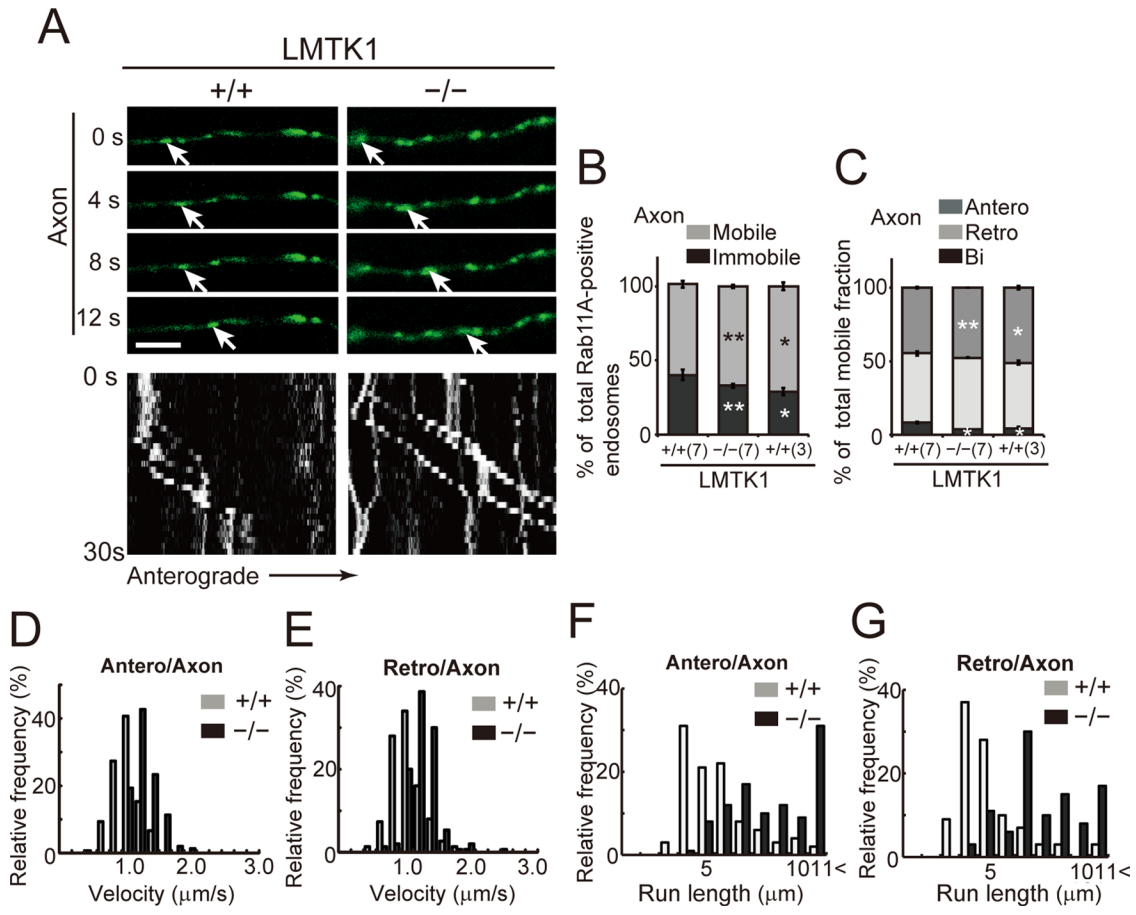

FIGURE 5: Dynamics of Rab11A-positive endosomes in axons of LMTK1$^{-/-}$ neurons. (A) Movement of Rab11A-positive endosomes in axons of LMTK1$^{+/+}$ or LMTK1$^{-/-}$ neurons. Typical anterograde movement of a Rab11A-positive endosome is indicated with arrows. The cell body is on the left side. Bottom, kymographs of Rab11A-positive endosomes moving in axon. Bar, 5 μm. (B) Percentage of moving (light gray) or stationary (dark gray) Rab11A-positive endosomes at 3 DIV (3) and 7 DIV (7) in axons. (C) Percentage of Rab11A-positive vesicles moving anterogradely (gray), retrogradely (light gray), and bidirectionally (dark gray) in axons of LMTK1$^{+/+}$ or LMTK1$^{-/-}$ neurons (n = 305 endosomes for LMTK1$^{+/+}$ and n = 301 endosomes for LMTK1$^{-/-}$). (D, E) Velocity of Rab11A-positive endosomes in axons. Relative frequency of Rab11A-positive endosomes moving at the indicated velocities in the anterograde (D) or retrograde (E) direction (n = 150 endosomes each for LMTK1$^{+/+}$ and LMTK1$^{-/-}$). (F, G) Run length of Rab11A-positive endosomes in LMTK1$^{+/+}$ or LMTK1$^{-/-}$ neurons. Relative frequency of Rab11A-positive endosomes moving at the indicated run length in the anterograde (F) or retrograde (G) direction (n = 100 endosomes each for LMTK1$^{+/+}$ and LMTK1$^{-/-}$). Data are the mean ± SEM of three independent experiments (*p < 0.05, **p < 0.01, Student's t test).

neurons (Figure 8B). The number of dendrites and branches and the total primary dendrite length were significantly increased in neurons expressing LMTK1-S34A (Figure 8, C–E). Sholl analysis revealed an increased number of crossings at both proximal (40 μm) and distal (280 μm) sites in LMTK1-S34A–expressing neurons compared with those expressing LMTK1-S34D or LMTK1-WT (Figure 8F). These results indicate that Cdk5, by phosphorylating Ser-34 of LMTK1, also regulates the effect of LMTK1 on dendritic arborization.

DISCUSSION

Down-regulation of LMTK1 induced longer dendrites with increased numbers of branches, indicating that LMTK1 suppresses dendrite growth and arborization. This activity of LMTK1 was mediated by Rab11A. Rab11A movements correlated well with the growth and branching of dendrites. The prevalence, speed, and run length of the outward movements of Rab11A-positive endosomes increased upon knockdown or knockout of LMTK1 in neurons to levels observed for endosomes that have incorporated caRab11A-Q70L; that is, Rab11A is highly active in the absence of LMTK1, and thus LMTK1 seems to maintain somewhat low levels of Rab11A activity. This is consistent with our previous results showing that LMTK1$^{-/-}$ mouse brains have higher levels of active Rab11A (Takano *et al.*, 2012). Indeed, premature outgrowth of dendrites in the LMTK1$^{-/-}$ brain was observed at early postnatal days, and thus LMTK1 could prevent dendritic hyperplasia by regulating membrane supply. LMTK1 function may therefore be important for establishing proper neuronal connections during brain development. It may be worth mentioning the current idea that premature or accelerated neuronal growth could be a cellular or molecular mechanism of autism spectrum disorder (Chomiak and Hu, 2013). It would be interesting to analyze the cytoarchitecture of autism-related brain regions, as well as behaviors, of LMTK1$^{-/-}$ mice.

Rab11 is a general marker of recycling endosomes (Ullrich *et al.*, 1996; Sonnichsen *et al.*, 2000). In neurons, Rab11 is suggested to

Axons or dendrites	Mobile (%)	Immobile (%)	Anterograde movement (%)	Retrograde movement (%)	Bidirectional movement (%)	Velocity (μm/s)	
						Anterograde	Retrograde
			LMTK1$^{+/+a}$				
Axons (3 D)	71 ± 2.5	29 ± 2. 5	51 ± 1.2	45 ± 10.2	4 ± 0.1	0.75 ± 0.03	0.71 ± 0.03
Axons (7 D)	60 ± 3.4	40 ± 2.2	45 ± 0.5	47 ± 10.5	8 ± 1.3	0.85 ± 0.04	0.92 ± 0.03
Dendrites	78 ± 1.8	22 ± 1.8	37 ± 1.2	31 ± 1.7	32 ± 1.3	0.94 ± 0.03	0.86 ± 0.03
			LMTKT$^{-/-b}$				
Axons (3 D)	80 ± 3.4	20 ± 3.4	58 ± 10.9	40 ± 10.9	2 ± 0.3	1.2 ± 0.02	1.11 ± 0.01
Axons (7 D)	67 ± 1.3	33 ± 1.3	48 ± 0.1	48 ± 0.3	4 ± 0.3	1.18 ± 0.02	1.15 ± 0.03
Dendrites	89 ± 10.2	11 ± 10.2	47 ± 0.5	19 ± 0.8	34 ± 0.9	1.24 ± 0.17	1.03 ± 0.05
			LMTK1$^{+/+c}$				
wtRab11A	81 ± 2.0	19 ± 2.0	41 ± 0.6	33 ± 2.0	26 ± 1.4	0.85 ± 0.04	0.85 ± 0.02
caRab11A[d]	85 ± 1.7	15 ± 1.7	49 ± 2.7	35 ± 0.7	15 ± 2.4	0.99 ± 0.02	0.96 ± 0.02
dnRab11A[e]	22 ± 4.2	78 ± 4.2	ND	ND	ND	ND	ND

Values are given as mean ± SEM. The original data are shown in Figures 4 and 5. See legends of Figures 4 and 5 for the number of samples. ND, not determined.
[a]Axons at 3 and 7 DIV and secondary dendrites at 7 DIV in LMTK1$^{+/+}$ mouse neurons.
[b]Axons at 3 and 7 DIV and secondary dendrites at 7 DIV in LMTK1$^{-/-}$ mouse neurons.
[c]Primary dendrites of LMTK1$^{+/+}$ neurons.
[d]Rab11A-Q70L.
[e]Rab11A-S25N.

TABLE 2: The movements of Rab11A-positive endosomes in axons or dendrites.

participate in the trafficking of synaptic vesicles in presynaptic regions, endocytic vesicles containing AMPA receptors in postsynaptic regions, and recycling endosomal vesicles in axons (Park *et al.*, 2004; Brown *et al.*, 2007; Ascano *et al.*, 2009; Takano *et al.*, 2012). Here we added dendritic growth and arborization as functions of Rab11A. The dynamics of Rab11-positive endosomes was only recently analyzed in detail in axons (Ascano *et al.*, 2009; Eva *et al.*, 2010), and no data are available for other regions of neurons. We have now analyzed trafficking of Rab11A-positive endosomes by real-time imaging in three regions of neurons, namely the cell body, dendritic shaft, and growth cone; in each region, LMTK1 down-regulation increased the dynamics of Rab11A-positive endosomes.

The movement of Rab11A-positive endosomes in dendrites was compared with that in axons. This was particularly interesting because the polarity of microtubules, along which endosomal vesicles are transported, differs between axons and dendrites—all microtubules are plus-end distal in axons, and microtubules of opposite polarity run parallel to each other in dendrites (Baas *et al.*, 1988; Stepanova *et al.*, 2003). It is unclear which polarity of microtubules serves as the track for vesicle transport in dendrites. We attempted to determine the types of movements in dendrites by comparing to those in axons. Rab11A-positive endosomes moved distally (anterogradely) and proximally (retrogradely) at a rate of 0.7–1.2 μm/s in dendrites, which was similar to movement in axons in this study and comparable to the rates of 0.4–1.2 μm/s in axons or neurites reported by others (Ascano *et al.*, 2009; Eva *et al.*, 2010; Power *et al.*, 2012). The rate was also similar to that estimated with caRab11A-Q70L–positive endosomes. These results indicate that moving endosomes are mostly loaded with the active Rab11A-GTP, but the data do not provide insight into the polarity of microtubules used for dendritic transport. One of the main differences we observed was in the percentage of bidirectional movement, which was 32–34% in dendrites and 4–8% in axons. A large portion of the bidirectional movement in dendrites may reflect frequent exchange of Rab11A-positive endosomes between microtubules having opposite polarity. In addition, these results may suggest that Rab11A-positive endosomes use mainly plus-end-distal microtubules for vesicle transport even in dendrites, because LMTK1 knockout did not increase the prevalence of retrograde transport of Rab11A-positive endosomes in dendrites (Table 2).

The prevalence of anterograde movement of wtRab11A-positive endosomes in LMTK1$^{+/+}$ neurons increased in LMTK1$^{-/-}$ neurons to levels observed with caRab11A-Q70L-labeled vesicles in LMTK1$^{+/+}$ neurons. How does reduced LMTK1 activity increase the prevalence of anterograde movement? Anterograde movement in axons should be driven by the plus-end motor, kinesin. Rab11 effectors such as Rip11/FIP5, Rab11-FIP3, and protrudin interact with the kinesins KIF3 and KIF5 (Schonteich *et al.*, 2008; Simon and Prekeris, 2008; Matsuzaki *et al.*, 2011). Down-regulation of LMTK1 up-regulates Rab11A activity (Takano *et al.*, 2012), which in turn would be expected to increase the number of interactions between the Rab11A effectors and kinesin, leading to anterograde-biased movement. Another issue is how recycling endosomes travel longer distances in LMTK1$^{-/-}$ axons and dendrites. Up-regulation of Rab11A activity increases endosomal vesicle budding (Jedd *et al.*, 1997; Takahashi *et al.*, 2012), which would be expected to result in smaller endosomal vesicles. The caRab11A-Q70L–positive endosomes were indeed smaller than wtRab11A endosomes. We observed greater dynamics among smaller endosomes compared with larger endosomes. This was also the case in LMTK1$^{-/-}$ neurons. We observed frequent budding of Rab11A-positive endosomes at the perinuclear endosomal compartment, and those endosomes were smaller than those in LMTK1$^{+/+}$ neurons. Small endosomes may experience less resistance than larger endosomes when they pass through bundles of microtubules, similar to mitochondrial transport in axons (Shahpasand *et al.*, 2012). Further, compared with larger vesicles, these smaller endosomal vesicles would have a greater density of active Rab11A on their surface, implying that the consequent greater

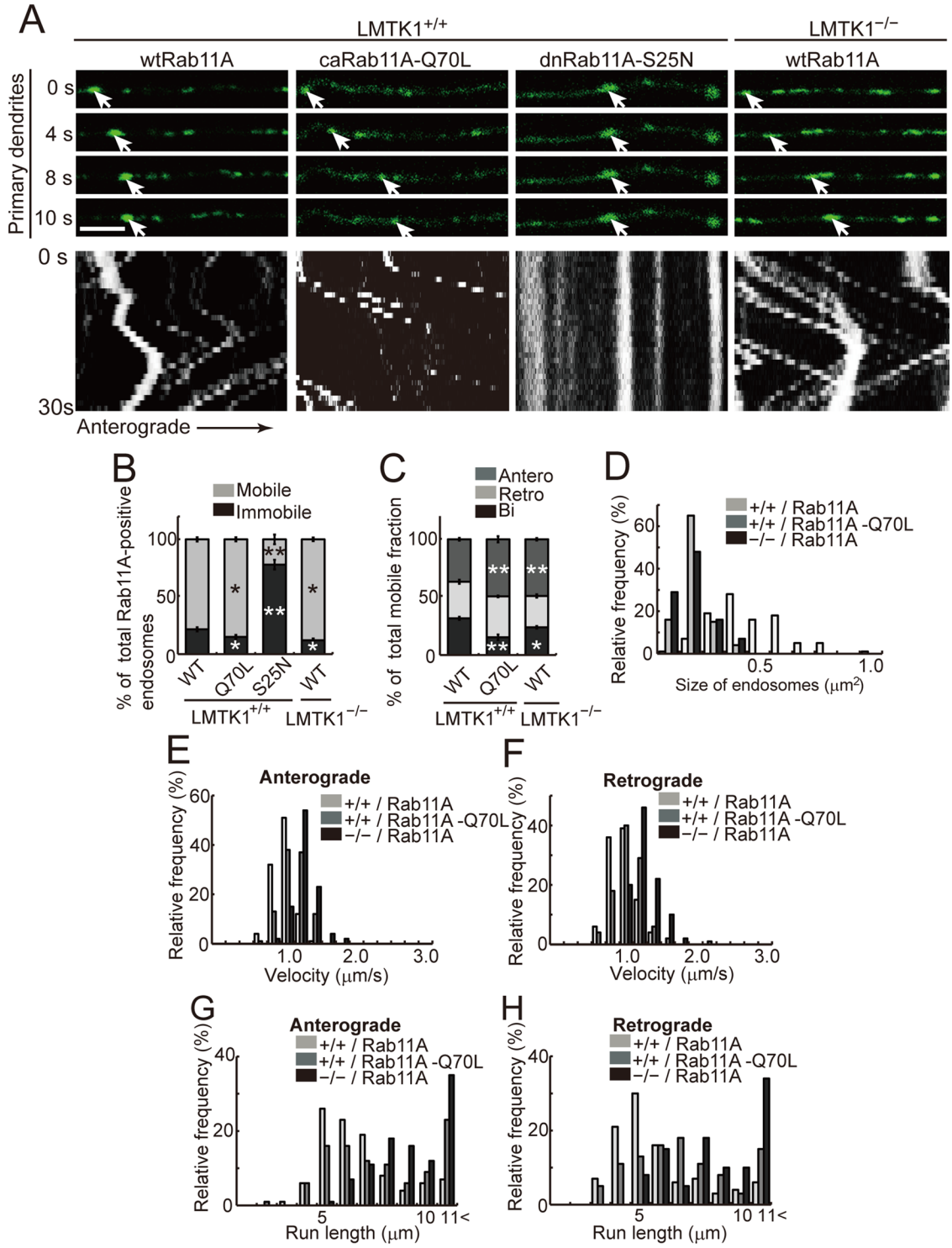

FIGURE 6: Movement of caRab11A-Q70L–positive endosomes in LMTK1$^{+/+}$ neurons and wtRab11A-positive endosomes in LMTK1$^{-/-}$ neurons. (A) A plasmid encoding EGFP-wtRab11A, EGFP-caRab11A-Q70L, or EGFP-dnRab11A-S25N was transfected into LMTK1$^{+/+}$ neurons, and movement of the Rab11A-positive endosomes was analyzed. Sequential frames over 10 s are shown in dendrites of LMTK1$^{+/+}$ neurons. Right, EGFP-Rab11A transfected into LMTK1$^{-/-}$ neurons. The cell body is to the left. The movement of typical Rab11A-positive endosomes is indicated with arrows. Bottom, kymographs of Rab11A-positive endosomes moving in dendrites. (B) Percentage of moving (light gray) or stationary (dark gray) Rab11A-positive endosomes in dendrites. (C) Percentage of Rab11A-positive endosomes moving anterogradely (gray), retrogradely (light gray), or bidirectionally (dark gray) in dendrites (n = 347 endosomes for LMTK1$^{+/+}$ neurons expressing wtRab11A, n = 349 endosomes for LMTK1$^{+/+}$ neurons expressing caRab11A-Q70L, n = 174 endosomes for LMTK1$^{+/+}$ neurons expressing dnRab11A-S25N, and n = 329 endosomes for LMTK1$^{-/-}$ neurons expressing wtRab11A). (D) The size of Rab11A-positive endosomes in primary dendrites. Relative frequency of Rab11A-positive endosomes of the indicated sizes. (E, F) The velocity of Rab11A-positive endosomes in primary

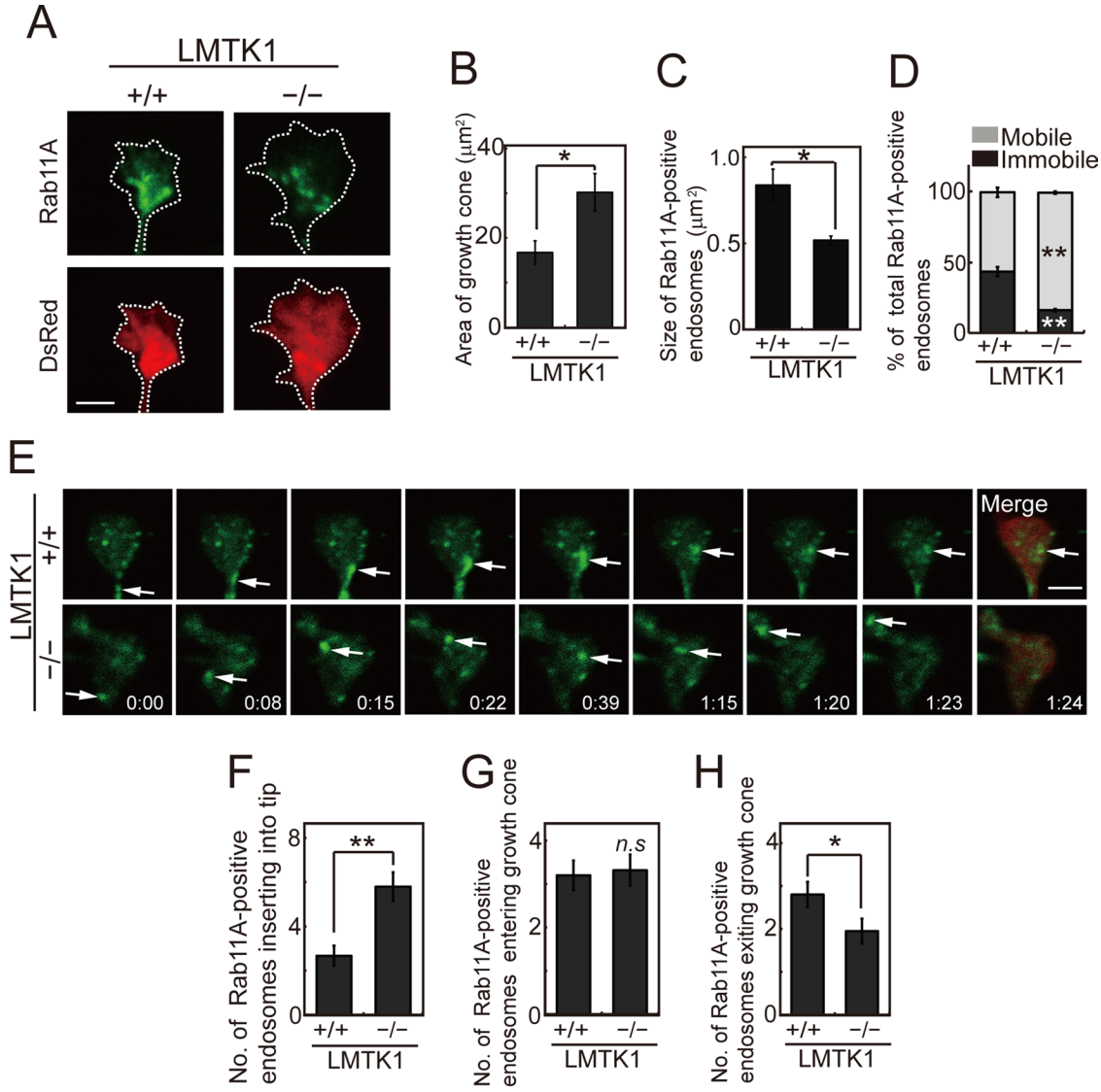

FIGURE 7: Movement of Rab11A-positive endosomes in growth cones of LMTK1$^{+/+}$ or LMTK1$^{-/-}$ neurons. (A) Growth cone of cortical neurons, which were prepared from LMTK1$^{+/+}$ (left) or LMTK1$^{-/-}$ (right) mouse brains cotransfected with a plasmid encoding EGFP-Rab11A (top) or DsRed (bottom) at 6 DIV. Rab11A-positive endosomes were observed at 7 DIV. Bar, 2.5 μm. (B) The growth cone area of LMTK1$^{+/+}$ or LMTK1$^{-/-}$ neurons (n = 30 each for LMTK1$^{+/+}$ or LMTK1$^{-/-}$ neurons). (C) The size of Rab11A-positive recycling endosomes in growth cones of LMTK1$^{+/+}$ or LMTK1$^{-/-}$ neurons (n = 30 endosomes each). (D) Percentage of mobile (light gray) or stationary (dark gray) Rab11A-positive endosomes in growth cones (n = 321 endosomes in LMTK1$^{+/+}$ neurons and n = 250 endosomes in LMTK1$^{-/-}$ neurons). (E) Movement of Rab11A-positive endosomes in growth cones of LMTK1$^{-/-}$ or LMTK1$^{+/+}$ neurons. Neurons prepared from LMTK1$^{+/+}$ (top) or LMTK1$^{-/-}$ (bottom) mouse brains were cotransfected with a plasmid encoding EGFP-Rab11A or DsRed. Movements of Rab11A-positive endosomes were analyzed with real-time imaging. Sequential frames are shown over 84 s for LMTK1$^{+/+}$ (top) and LMTK1$^{-/-}$ (bottom). The movement of a typical Rab11A-positive endosome is indicated with arrows. (F–H) The number of Rab11A-positive endosomes that were inserted into the plasma membrane at the tip of the growth cone (F), entered the growth cone from the dendritic shaft (G), or exited the growth cone (H) over 160 s (n = 165 endosomes in LMTK1$^{+/+}$ neurons and n = 185 endosomes in LMTK1$^{-/-}$ neurons). Data are the mean ± SEM of three independent experiments (*p < 0.05; **p < 0.01; n.s., not significant, Student's t test).

dendrites. Relative frequency of Rab11A-positive endosomes moving at the indicated velocities in the anterograde (E) or retrograde (F) direction (n = 150 endosomes each for LMTK1$^{+/+}$ neurons expressing wtRab11A or caRab11A-Q70L and LMTK1$^{-/-}$ neurons expressing wtRab11A). (G, H) Run length of wtRab11A, caRab11A-Q70L–positive endosomes in LMTK1$^{+/+}$ neurons, and Rab11A-positive endosomes in LMTK1$^{-/-}$ neurons. Relative frequency of Rab11A-positive endosomes moving at the indicated run length in the anterograde (G) or retrograde (H) direction (n = 100 endosomes each for LMTK1$^{+/+}$ neurons expressing wtRab11A or caRab11A-Q70L, and LMTK1$^{-/-}$ neurons expressing wtRab11A). Data are the mean ± SEM of three independent experiments (*p < 0.05, **p < 0.01, Student's t test).

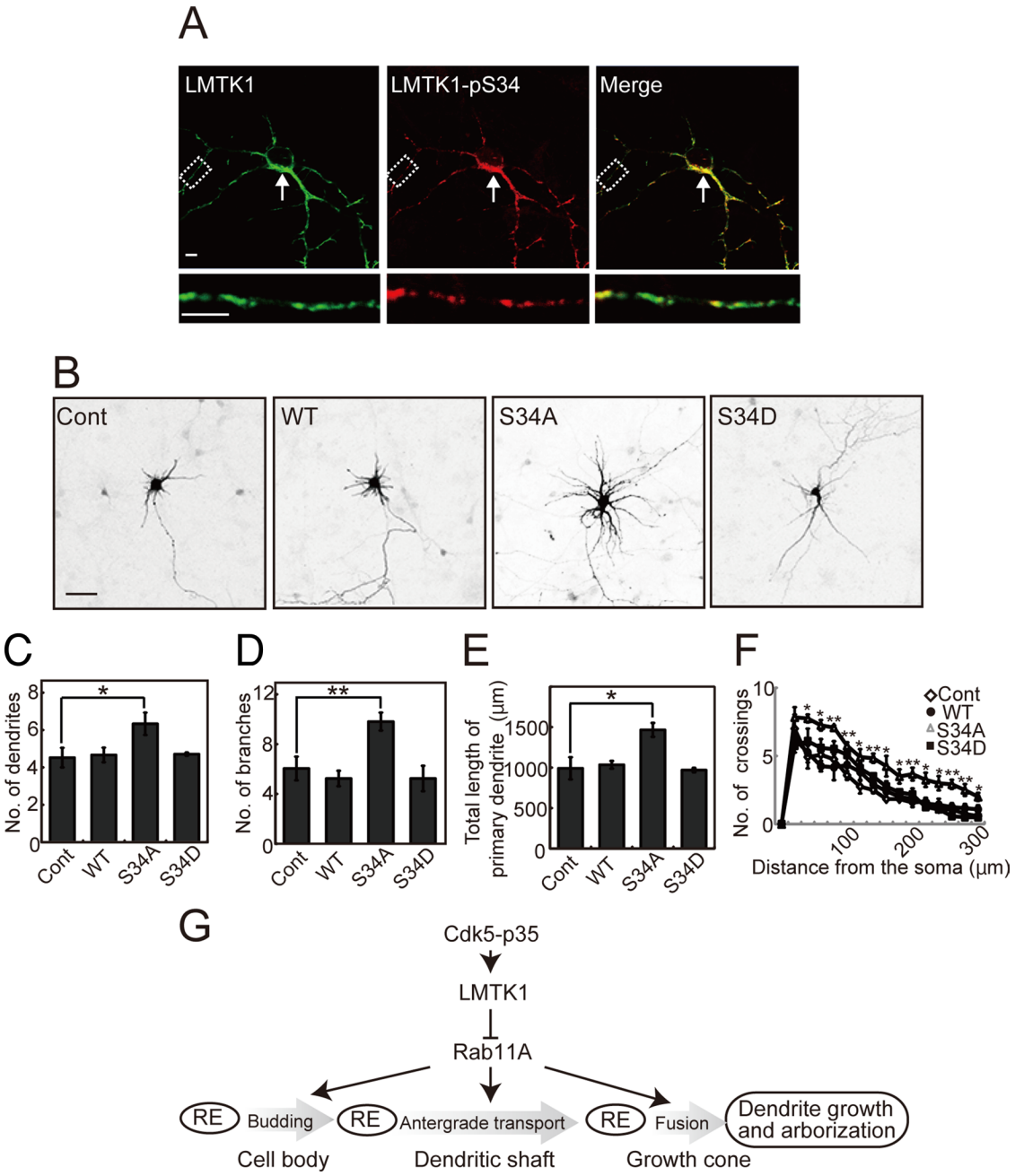

FIGURE 8: Nonphosphorylatable mutant S34A of LMTK1 enhances dendritic arborization. (A) Immunofluorescence staining of primary cortical neurons with anti-pS34. Cortical neurons expressing LMTK1-myc were double labeled with anti-myc (left) and anti-pS34 (middle). Right, merged images. Bottom, higher-magnification views of dendrites. Bar, 5 μm. (B) Effect of LMTK1-Ser34 mutants on dendritic arborization. A plasmid encoding LMTK1-WT, -S34A, or -S34D was cotransfected into cortical neurons along with DsRed at 0 DIV, and images of DsRed are shown at 7 DIV. Bar, 50 μm. (C–E) The number of dendrites (C) or branches (D) and total length of the primary dendrite (E) in the LMTK1-expressing neurons ($n = 21$ each). (F) Sholl analysis of neurons transfected with a plasmid encoding LMTK1-WT, -S34A, or -S34D ($n = 12$ each). Data are the mean ± SEM of three independent experiments (*$p < 0.05$, **$p < 0.01$, Student's t test). (G) Scheme representing the role of LMTK1 in dendrite formation. Cdk5 regulates LMTK1 by phosphorylation at Ser-34. LMTK1 inhibits Rab11A activity, which promotes budding of endocytic vesicles in the cell body, their transport in dendritic shaft, and fusion in the growth cone. The Cdk5-LMTK1-Rab11A pathway is a regulatory mechanism for dendrite formation, as well as axon outgrowth, via membrane supply.

number of kinesin molecules on these small Rab11A-positive vesicles biases vesicle movement toward the anterograde direction. In this way, active Rab11A may sustain movement for a longer time, resulting in preferential anterograde movement.

Cdk5-p35 phosphorylates LMTK1 at Ser-34 upstream of the kinase domain (Takano *et al.*, 2010; Tsutsumi *et al.*, 2010), and expression of the nonphosphorylatable mutant of LMTK1, S34A, led to increased Rab11A-positive endosome movement, axonal

outgrowth, and dendrite growth and arborization. These results indicate that the Cdk5-LMTK1-Rab11A pathway operates during the process of supplying membrane materials to neurites. Indeed, Cdk5 has been reported to have a function in membrane transport. In axons of *Caenorhabditis elegans*, the trafficking of synaptic vesicles is stimulated in Cdk5 mutants (Ou *et al.*, 2010; Goodwin *et al.*, 2012), consistent with our results. Although there are no reports on Cdk5 function in endosomal transport in mammalian neurons, involvement of Cdk5 in dendrite formation has been documented. Layer V pyramidal neurons in cerebral cortex fail to develop a normal apical dendrite and instead extend multiple lateral dendrites in $Cdk5^{-/-}$ mouse brain (Ohshima *et al.*, 2007). Knockdown or knockout of Cdk5 in hippocampal neurons suppresses the brain-derived neurotrophic factor–induced increase in primary dendrites (Cheung *et al.*, 2007). Cdk5 also affects dendrite formation by phosphorylating cytoskeletal proteins, different from that observed here through membrane traffic. Collapsin response mediator proteins (CRMPs) 1 and 2 are microtubule-associated proteins that are phosphorylated at Ser-522 by Cdk5 (Uchida *et al.*, 2005). Double-mutant $crmp2^{ki/ki}$ (knock-in mutant of Ser522Ala) and $crmp1^{-/-}$ induce an irregular curling dendritic phenotype without changing the number and branching of primary dendrites (Yamashita *et al.*, 2012). Cdk5 is a multifunctional protein kinase with action points in several signaling pathways, including neurotrophic factor–dependent signal transduction, cytoskeletal reorganization, and membrane trafficking (Dhavan and Tsai, 2001; Cheung and Ip, 2007; Hisanaga and Endo, 2010). Results different from the foregoing may be a consequence of differences in experimental systems. Of importance, axon and dendrite formation may be a result of integration of multiple Cdk5 actions.

MATERIALS AND METHODS

Antibodies

Anti-p35 (C-19), anti-Cdk5 (DC17), and monoclonal anti-myc (9E10) were purchased from Santa Cruz Biotechnology (Santa Cruz, CA). Anti-Rab11 was from Invitrogen (Carlsbad, CA). Monoclonal anti–neuron-specific class III β-tubulin was from Techne Corporation (Minneapolis, MN). Anti-actin was from Sigma-Aldrich (Saint Louis, MO). Anti-PSD95 was from Thermo Scientific (Manor Park Runcom, Cheshire, United Kingdom). Anti-GluR2 was from Chemicon (Temecula, CA). Anti-LMTK1 and anti–phospho-Ser34 of LMTK1 (pS34) have been described (Tsutsumi *et al.*, 2008, 2010). Alexa-conjugated secondary antibodies were from Invitrogen.

Plasmid construction

EmGFP-miRNAs against LMTK1 have been described (Takano *et al.*, 2012). The LMTK1 alanine (A) mutant and the phosphorylation-mimic aspartic acid (D) mutant at Ser-34 have been described (Takano *et al.*, 2010; Tsutsumi *et al.*, 2010). pEGFP-Rab5A, pEGFP-Rab7, pEGFP-Rab11A, pEGFP-Rab11A-Q70L, and pEGFP-Rab11A-S25N have been described (Fukuda, 2003; Fukuda *et al.*, 2008).

Primary cortical neuron cultures and transfection

ICR mice were obtained from Sankyo Laboratory Service (Tokyo, Japan). $LMTK1^{-/-}$ mice have been described (Takano *et al.*, 2012). Mice were housed in a temperature-controlled room under a 12-h light/12-h dark cycle with free access to food and water. All experiments were performed according to the guidelines for animal experimentation of Tokyo Metropolitan University. Brain cortices from embryonic day 17 or 18 mice were dissected and dissociated, and neurons were plated in polyethyleneimine (PE)-coated dishes or PE-coated glass coverslips at a density of 2.0×10^6 neurons/cm^2 (Saito *et al.*, 2007). Plasmid vectors were introduced into neurons with electroporation using an Amaxa Nucleofector apparatus (Lonza, Tokyo, Japan; Takano *et al.*, 2012).

Immunofluorescence staining and statistical analysis

Neurons were fixed with 4% paraformaldehyde in phosphate-buffered saline (PBS) for 20 min at room temperature and permeabilized in PBS containing 0.1% (wt/vol) Triton X-100 and 5% normal goat serum for 30 min. The cells were incubated with the indicated primary antibodies followed by secondary antibodies conjugated to Alexa 488, Alexa 546, or Alexa 647 (Invitrogen). Fluorescence images were acquired with an LSM 5 EXCITER confocal microscope or Zeiss LSM 710 confocal microscope (Carl Zeiss, Jena, Germany). The statistical significance of the data was evaluated with the Student's *t* test, $*p < 0.05$ and $**p < 0.01$.

Analysis of Rab11A-positive endosome dynamics in neurons

Mouse brain cortical neurons were plated on a polyethyleneimine-coated glass-bottom dish (CELLview; Greiner, Frickenhausen, Germany). Three or seven days after seeding, the culture medium was replaced with Neurobasal medium without phenol red and supplemented with B-27 (Invitrogen). The culture dish was mounted on a temperature-controlled stage on a Zeiss confocal microscope (LSM 710) at 37°C in 5% CO_2. Live images of vesicle movement were captured in dendrites or axons for at least 1 min with 1-s intervals using a 63× oil-immersion lens. Rab11A-positive endosome movement was analyzed for the proportion of moving or stationary endosomes, the direction of movement, and speed. Rab11A-positive endosomes were classified as mobile or immobile according to criteria described by Eva *et al.* (2010). Briefly, Rab11A-positive endosomes were classified as immobile when their movement was <2 µm during observation for 100 s. Rab11A-positive endosomes moving in both directions but with net movement of <2 µm were classified as bidirectional. Rab11A-positive endosomes with net movement >2 µm in either direction were classified as anterograde or retrograde. Rab11A-positive endosomes were tracked for 100 s, and the maximum distance moved during three scans (3 s) was measured using Zen software and used to calculate the speed. The run length covered by Rab11A-positive endosomes was measured as a single continuous movement over 20 scans (20 s). Apparent sizes of Rab11A-positive endosomes were estimated with Zen software based on the area of EGFP fluorescence. Kymographs were made from serial flames of the same area using MetaMorph software (Molecular Devices, Sunnyvale, CA).

Preparation of cell extracts and immunoblotting

Neurons were disrupted in RIPA buffer (20 mM Tris-HCl, pH 7.5, 150 mM NaCl, 1 mM ethylene glycol tetraacetic acid, 1 mM EDTA, 1% [wt/vol] Nonidet P-40, 0.1% SDS, 0.1% sodium deoxycholate, 0.4 mM Pefabloc, 10 µg/ml leupeptin, 10 mM NaF, 10 mM β-glycerophosphate, 1 mM Na_3VO_4). After centrifugation at 10,000 × *g* for 20 min at 4°C, the extract was suspended in SDS sample buffer and boiled for 5 min. SDS–PAGE and immunoblotting were performed as described (Takano *et al.*, 2010, 2012).

Golgi staining

$LMTK1^{+/+}$ or $LMTK1^{-/-}$ brain at postnatal day 7 or 3 mo of age was stained with reagents in an FD Rapid GolgiStain kit (FD Neurotechnologies, Columbia, MD).

ACKNOWLEDGMENTS

This work was supported in part by Grants-in-Aid for Scientific Research from the Japan Society for the Promotion of Science (T.T.) and the Ministry of Education, Culture, Sports, Science, and Technology of Japan (S.H.).

REFERENCES

Arimura N, Kaibuchi K (2007). Neuronal polarity: from extracellular signals to intracellular mechanisms. Nat Rev Neurosci 8, 194–205.

Ascano M, Richmond A, Borden P, Kuruvilla R (2009). Axonal targeting of Trk receptors via transcytosis regulates sensitivity to neurotrophin responses. J Neurosci 29, 11674–11685.

Baas PW, Deitch JS, Black MM, Banker GA (1988). Polarity orientation of microtubules in hippocampal neurons: uniformity in the axon and nonuniformity in the dendrite. Proc Natl Acad Sci USA 85, 8335–8339.

Baker SJ, Sumerson R, Reddy CD, Berrebi AS, Flynn DC, Reddy EP (2001). Characterization of an alternatively spliced AATYK mRNA: expression pattern of AATYK in the brain and neuronal cells. Oncogene 20, 1015–1021.

Bellon A (2007). New genes associated with schizophrenia in neurite formation: a review of cell culture experiments. Mol Psychiatry 12, 620–629.

Brown TC, Correia SS, Petrok CN, Esteban JA (2007). Functional compartmentalization of endosomal trafficking for the synaptic delivery of AMPA receptors during long-term potentiation. J Neurosci 27, 13311–13315.

Cheung ZH, Chin WH, Chen Y, Ng YP, Ip NY (2007). Cdk5 is involved in BDNF-stimulated dendritic growth in hippocampal neurons. PLoS Biol 5, e63.

Cheung ZH, Ip NY (2007). The roles of cyclin-dependent kinase 5 in dendrite and synapse development. Biotechnol J 2, 949–957.

Chomiak T, Hu B (2013). Alterations of neocortical development and maturation in autism: insight from valproic acid exposure and animal models of autism. Neurotoxicol Teratol 36, 57–66.

Dhavan R, Tsai LH (2001). A decade of CDK5. Nat Rev Mol Cell Biol 2, 749–759.

Eva R, Dassie E, Caswell PT, Dick G, ffrench-Constant C, Norman JC, Fawcett JW (2010). Rab11 and its effector Rab coupling protein contribute to the trafficking of beta 1 integrins during axon growth in adult dorsal root ganglion neurons and PC12 cells. J Neurosci 30, 11654–11669.

Fukuda M (2003). Distinct Rab binding specificity of Rim1, Rim2, rabphilin, and Noc2. Identification of a critical determinant of Rab3A/Rab27A recognition by Rim2. J Biol Chem 278, 15373–15380.

Fukuda M, Kanno E, Ishibashi K, Itoh T (2008). Large scale screening for novel rab effectors reveals unexpected broad Rab binding specificity. Mol Cell Proteomics 7, 1031–1042.

Goodwin PR, Sasaki LM, Juo P (2012). Cyclin-dependent kinase 5 regulates the polarized trafficking of neuropeptide-containing dense-core vesicles in *Caenorhabditis elegans* motor neurons. J Neurosci 13, 8158–8172.

Hisanaga S, Endo R (2010). Regulation and role of cyclin-dependent kinase activity in neuronal survival and death. J Neurochem 115, 1309–1321.

Jedd G, Mulholland J, Segev N (1997). Two new Ypt GTPases are required for exit from the yeast *trans*-Golgi compartment. J Cell Biol 137, 563–580.

Kawauchi T, Sekine K, Shikanai M, Chihama K, Tomita K, Kubo K, Nakajima K, Nabeshima Y, Hoshino M (2010). Rab GTPases-dependent endocytic pathways regulate neuronal migration and maturation through N-cadherin trafficking. Neuron 67, 588–602.

Matsuzaki F, Shirane M, Matsumoto M, Nakayama KI (2011). Protrudin serves as an adaptor molecule that connects KIF5 and its cargoes in vesicular transport during process formation. Mol Biol Cell 22, 4602–4620.

Ohshima T *et al*. (2007). Cdk5 is required for multipolar-to-bipolar transition during radial neuronal migration and proper dendrite development of pyramidal neurons in the cerebral cortex. Development 134, 2273–2282.

Ou CY *et al*. (2010). Two cyclin-dependent kinase pathway are essential for polarized trafficking of presynaptic components. Cell 141, 846–858.

Pardo CA, Eberhart CG (2007). The neurobiology of autism. Brain Pathol 17, 434–447.

Park M, Penick EC, Edwards JG, Kauer JA, Ehlers MD (2004). Recycling endosomes supply AMPA receptors for LTP. Science 305, 1972–1975.

Power D, Srinivasan S, Gunawardena S (2012). In-vivo evidence for the disruption of Rab11 vesicle transport by loss of huntingtin. Neuroreport 23, 970–977.

Ren M, Xu G, Zeng J, De Lemos-Chiarandini C, Adesnik M, Sabatini DD (1998). Hydrolysis of GTP on rab11 is required for the direct delivery of transferrin from the pericentriolar recycling compartment to the cell surface but not from sorting endosomes. Proc Natl Acad Sci USA 95, 6187–6192.

Saito T, Konno T, Hosokawa T, Asada A, Ishiguro K, Hisanaga S (2007). p25/cyclin-dependent kinase 5 promotes the progression of cell death in nucleus of endoplasmic reticulum-stressed neurons. J Neurochem 102, 133–140.

Sann S, Wang Z, Brown H, Jin Y (2009). Roles of endosomal trafficking in neurite outgrowth and guidance. Trends Cell Biol 19, 317–324.

Schonteich E, Wilson GM, Burden J, Hopkins CR, Anderson K, Goldenring JR, Prekeris R (2008). The Rip11/Rab11-FIP5 and kinesin II complex regulates endocytic protein recycling. J Cell Sci 121, 3824–3833.

Shahpasand K, Uemura I, Saito T, Asano T, Hata K, Shibata K, Toyoshima Y, Hasegawa M, Hisanaga S (2012). Regulation of mitochondrial transport and inter-microtubule spacing by tau phosphorylation at the sites hyperphosphorylated in Alzheimer's disease. J Neurosci 32, 2430–2441.

Shelly M, Poo MM (2011). Role of LKB1-SAD/MARK pathway in neuronal polarization. Dev Neurobiol 71, 508–527.

Simon GC, Prekeris R (2008). Mechanisms regulating targeting of recycling endosomes to the cleavage furrow during cytokinesis. Biochem Soc Trans 36, 391–394.

Sonnichsen B, De Renzis S, Nielsen E, Rietdorf J, Zerial M (2000). Distinct membrane domains on endosomes in the recycling pathway visualized by multicolor imaging of Rab4, Rab5, and Rab11. J Cell Biol 149, 901–914.

Stenmark H (2009). Rab GTPases as coordinators of vesicle traffic. Nat Rev Mol Cell Biol 10, 513–525.

Stepanova T *et al*. (2003). Visualization of microtubule growth in cultured neurons via the use of EB3-GFP (end-binding protein 3-green fluorescent protein). J Neurosci 23, 2655–2664.

Takahashi M, Murate M, Fukuda M, Sato SB, Ohta A, Kobayashi T (2007). Cholesterol controls lipid endocytosis through Rab11. Mol Biol Cell 18, 2667–2677.

Takahashi S, Kubo K, Waguri S, Yabashi A, Shin HW, Katoh Y, Nakayama K (2012). Rab11 regulates exocytosis of recycling vesicles at the plasma membrane. J Cell Sci 125, 4049–4057.

Takai Y, Sasaki T, Matozaki T (2001). Small GTP-binding proteins. Physiol Rev 81, 153–208.

Takano T, Tomomura M, Yoshioka N, Tsutsumi K, Terasawa Y, Saito T, Kawano H, Kamiguchi H, Fukuda M, Hisanaga S (2012). LMTK1/AATYK1 is a novel regulator of axonal outgrowth that acts via Rab11 in a Cdk5-dependent manner. J Neurosci 32, 6587–6599.

Takano T, Tsutsumi K, Saito T, Asada A, Tomomura M, Fukuda M, Hisanaga S (2010). AATYK1A phosphorylation by Cdk5 regulates the recycling endosome pathway. Genes Cells 15, 783–797.

Tomomura M, Morita N, Yoshikawa F, Konishi A, Akiyama H, Furuichi T, Kamiguchi H (2007). Structural and functional analysis of the apoptosis-associated tyrosine kinase (AATYK) family. Neuroscience 148, 510–521.

Tsutsumi K, Takano T, Endo R, Fukuda M, Ohshima T, Tomomura M, Hisanaga S (2010). Phosphorylation of AATYK1 by Cdk5 suppresses its tyrosine phosphorylation. PLoS One 5, e10260.

Tsutsumi K, Tomomura M, Furuichi T, Hisanaga S (2008). Palmitoylation-dependent endosomal localization of AATYK1A and its interaction with Src. Genes Cells 13, 949–964.

Uchida Y *et al*. (2005). Semaphorin3A signalling is mediated via sequential Cdk5 and GSK3beta phosphorylation of CRMP2: implication of common phosphorylating mechanism underlying axon guidance and Alzheimer's disease. Genes Cells 10, 165–179.

Ullrich O, Reinsch S, Urbe S, Zerial M, Parton RG (1996). Rab11 regulates recycling through the pericentriolar recycling endosome. J Cell Biol 135, 913–924.

Yamashita N, Ohshima T, Nakamura F, Kolattukudy P, Honnorat J, Mikoshiba K, Goshima Y (2012). Phosphorylation of CRMP2 (collapsin response mediator protein 2) is involved in proper dendritic field organization. J Neurosci 32, 1360–1365.

Yap CC, Winckler B (2012). Harnessing the power of the endosome to regulate neural development. Neuron 74, 440–451.

Zerial M, McBride H (2001). Rab proteins as membrane organizers. Nat Rev Mol Cell Biol 2, 107–117.